HHS Public Access

Author manuscript

FASEB J. Author manuscript; available in PMC 2020 August 21.

Published in final edited form as:

FASEB J. 2020 May ; 34(5): 6741–6756. doi:10.1096/fj.201902838R.

Ciliary IFT80 is essential for intervertebral disc development and maintenance

Xinhua Li[1,2], **Shuting Yang**[1], **Lin Han**[3], **Keya Mao**[4], **Shuying Yang**[1,5,*]

[1]Department of Department of Basic and Translational Science, School of Dental Medicine, University of Pennsylvania, Philadelphia, PA 19104, USA

[2]Department of Spinal Surgery, East Hospital, Tongji University, School of Medicine, Shanghai 200120, China

[3]School of Biomedical Engineering, Science and Health Systems, Drexel University, Philadelphia, PA 19104, USA

[4]Department of Orthopaedics, Chinese PLA General Hospital (301 Hospital), Beijing 100853, China

[5]The Penn Center for Musculoskeletal Disorders, School of Medicine, University of Pennsylvania, Philadelphia, PA 19104, USA

Abstract

The intervertebral disc degeneration (IVDD) related diseases occur in more than 90% of the population older than 50 years. Owing to the lack of understanding of the cellular mechanisms involved in IVDD formation effective treatment options are still unavailable. Primary cilia are microtubule-based organelles that play important roles in organ development. Intraflagellar transport (IFT) proteins are essential for the assembly and bidirectional transport within the cilium. Role of cilia and IFT80 protein in intervertebral disc (IVD) development, maintenance and degeneration are largely unknown. Using cilia-GFP mice, we found presence of cilia on growth plate (GP), cartilage endplate (EP) annulus fibrosus (AF) and nucleus pulposus (NP) with varying ciliary length. Cilia length in NP and AF during IVDD were significantly decreased. However, cilia numbers increased by 63% in AF during repair. Deletion of IFT80 in type II collagen-positive cells resulted in cilia loss in GP and EP, and disrupted IVD structure with disorganized and decreased GP, EP and internal AF (IAF), and less compact and markedly decreased gel-like matrix in the NP. Deletion of IFT80 in type I collagen-positive cells led to a disorganized outer AF (OAF) with thinner, loosened and disconnected fiber alignment. Mechanistic analyses showed that loss of IFT80 caused a significant increase in cell apoptosis in the IVD, and a marked decrease in expression of chondrogenic markers - type II collagen, sox9, aggrecan, and hedgehog (Hh)

*Corresponding author: Dr. Shuying Yang, shuyingy@upenn.edu, Department of Basic and Translational Science, School of Dental Medicine, University of Pennsylvania, 240 South 40th Street, Levy 437, Philadelphia, PA 19104-6030, Phone: (215) 898-2685, Fax: (215) 573-2324, shuyingy@upenn.edu.

Author contributions

XL, SY, and LH performed the experiments, interpreted the data and wrote the initial draft of the manuscript. STY managed mice colonies and assisted with the experiments. SY conceived, supervised the study and wrote the manuscript. LH and KM provided critical suggestions, reagents and technical assistance during the study.

Conflict of interest

The authors declare no conflict of interest.

signaling components, including Gli1 and Patch1 in the IVD of IFT80$^{fl/fl}$; Col2-creERT mice, and Gli1 and Patch1 expression in the OAF of IFT80$^{fl/fl}$; Col1-creERT mice. Interestingly, Smoothened agonist-SAG rescued OAF cell proliferation and osteogenic differentiation. Our findings demonstrate that ciliary IFT80 is important for the maintenance of IVD cell organization and function through regulating cell survival and Hh signaling.

Keywords

Primary cilia; IFT80; Intervertebral disc degeneration; Nucleus pulposus; Annulus fibrosus

Introduction

Intervertebral disc degeneration (IVDD) related diseases occur in more than 90% of the population older than 50 years(1). The annual cost of IVDD related disease treatment is over $100 billion in the US alone, which is even more than the total cost of treating stroke, respiratory infection, diabetes, coronary artery disease, and rheumatoid disease(2, 3). Currently available treatments only provide symptomatic relief from pain through physical therapy, and activity modification or surgical intervention (4–6), such as disc decompression and spinal fusion. These interventions cannot decelerate or prevent the progression of degeneration or restore physiological function of the intervertebral disc (IVD). Understanding the exact etiology is the key to cure this disease. A variety of risk factors, such as excessive mechanical overload, aging, tissue injury, smoking and genetic risk, have been found to contribute to the onset and progression(7). Among these factors, abnormal mechanical loading has been regarded as one of the major factors causing IVDD(7). Although the mechanism by which mechanical loads alter cell behaviors in IVD is still unknown, studies from bone and cartilage, and kidneys have demonstrated that primary cilia play critical roles during cell mechano-sensation and mechano-transduction (8–10).

Primary cilia are highly conserved microtubule-based organelles that project from the cell surface into the extracellular environment and play important roles in mechano-sensation, mechano-transduction, polarity maintenance, and cell behaviors during organ development and pathological changes, including in the musculoskeletal system (9, 11). The assembly and function of cilia require effective intraflagellar transport (IFT) of the IFT particles and proteins in the cilium, which is a bidirectional transport operated by IFT protein complexes and IFT motors. IFT protein complexes are divided into complex A and complex B, which contain 20 IFT proteins. IFT complex A regulates the retrograde IFT of the proteins from the ciliary tip to the base, while IFT complex B is involved in anterograde IFT of the proteins from the base to the ciliary tip (9). IFT80 is one of the IFT complex B proteins. Some studies have reported that cells with cilia defects in bone, cartilage and kidneys cannot respond to mechano-stimulation from the environment, which causes numerous human diseases, including Jeune syndrome, Alkaptonuria, spinal scoliosis, osteoarthritis, and polycystic kidney disease (8, 10, 12–16). Our previous studies have demonstrated that IFT80 is important for primary cilia formation and ciliary-dependent hedgehog (Hh) signaling in postnatal cartilage and bone formation (12, 17, 18). However, roles of cilia and IFT80 in IVD development, maintenance and degeneration process are largely unknown.

In this study, to determine how cilia are distributed and arranged in the mouse IVD and whether cilia and IFT80 are involved in IVD development and function, we first analyzed primary cilia in each IVD compartment (an annulus fibrosus (AF), the growth plate (GP) and cartilage endplate (EP), and the nucleus pulposus (NP)) using a cilia-GFP reporter mouse model. To trace how primary cilia are modulated during IVD development and aging process, we analyzed the length and percentage of primary cilia in IVD components at postnatal day 0 (P0), 1Month (M), 3M, and 2-year-old mice by using cilia-GFP mouse model and at 1-week and 4-week following IVD injury. Furthermore, we generated mice with a specific deletion of IFT80 in the cartilage and outer AF (OAF) in IVD by crossing $IFT80^{fl/fl}$ mice with tamoxifen (TM) inducible type II collagen Cre (Col2-creERT) and type I collagen Cre (Col1-creERT) mice respectively. We further analyzed the function and mechanism of IFT80 and primary cilia in IVD formation and cell function by characterizing $IFT80^{fl/fl}$; Col2-creERT and $IFT80^{fl/fl}$; Col1-creERT mouse models. Our findings revealed that primary cilia and IFT80 control IVD formation and the maintenance of the microstructural pattern.

Methods & Materials

Mice

All procedures regarding housing, breeding, and collection of animal tissues were performed as per approved protocols by the Institutional Animal Care and Use Committee (IACUC) of the University of Pennsylvania, in accordance with the IACUC's relevant guidelines and regulations. All animals are of C57BL strain.

An $IFT80^{fl/fl}$ mouse model with two LoxP sites flanking exon 6 of IFT80 was generated as described previously (12). Cilia-GFP(19), Col2-creERT(20), and Col1-creERT(21) mice were purchased from Jackson laboratory (Bar Habor, ME, USA). To observe the percentage and length of primary cilia in each component tissue of IVD, we bred CMV-cre with Cilia-GFP mice to generate CMV-cilia-GFP mice with GFP expression in primary cilia. Col2-creERT; $IFT80^{fl/fl}$ or Col1-creERT; $IFT80^{fl/fl}$ mice were generated by breeding $IFT80^{fl/fl}$ mice with Col2-creERT or Col1-creERT mice. There was no significance difference in IVD development among Col2-creERT, Col1-creERT, wild-type and $IFT80^{fl/fl}$ mice, so $IFT80^{fl/fl}$ mice were used as control. The mice were injected with TM at indicated time points to delete IFT80. TM (T5648, Sigma) solution preparation and administration were performed as previously described (18). Briefly, TM was first dissolved in 100% ethanol (100 mg/mL) and then diluted with sterile corn oil to a final concentration of 10 mg/ml. For neonatal injections, Col2-creERT; $IFT80^{fl/fl}$, Col1-creERT; $IFT80^{fl/fl}$ and $IFT80^{fl/fl}$ mice were administered at postnatal day 3, 5, and 7 with the same dose of TM (75 mg TM/kg body weight). Mice were harvested at postnatal day 28. Three to six independent litters were analyzed. Col2-creERT; $IFT80^{fl/fl}$ mice and Col1-creERT; $IFT80^{fl/fl}$ mice were compared to age-matched $IFT80^{fl/fl}$ littermate controls.

Tail injury surgery

Young adult (8-week-old) C57BL/6J mice were used in this study. The tail injury surgery was performed as described previously (22). Briefly, under anesthesia, the mouse coccygeal

(Co) IVDs were injured by inserting a 26-G needle into IVD space until the needle tip reached 2/3 of the disc thickness under fluoroscopic guidance with a Faxitron MX-20 (Faxitron X-Ray). Coccygeal disc between the fifth and sixth coccygeal vertebrae (Co5/6) in each mouse were injured, whereas mouse Co6/7 without injury were served as intact controls (n=6 mice per group).

H&E staining and Safranin O/fast green staining

Mice IVD between the third and fifth lumbar spine tissues (L3-L5) were excised, fixed with 10% natural buffered formalin, and decalcified in 10% ethylenediaminetetraacetic acid (EDTA) for 10 days at 4 °C. The samples were embedded in paraffin. Using a standard microtome (RM2255, Leica), 6μm sections were prepared and stained with H&E. Safranin O/fast green staining was performed to visualize cartilage and assess proteoglycan content as described previously (18). Deparaffinized slides were stained with Weigert's iron hematoxylin and fast green, and then stained with 0.1% Safranin O solution. Three to six mice were evaluated in each group.

Immunofluorescence microscopy

Coronal disc tissue sections with 6μm thickness were deparaffinized and incubated either in microwaved citrate buffer for 20 min or with proteinase K (20μg/mL, D3001–2-5, Zymo Research) for 10 min at room temperature. Subsequently, sections were blocked in 5% normal serum (10000 C, Thermo Fisher Scientific) in PBS-T (0.4% Triton X-100 in PBS) or incubated with antibodies against type I collagen (1:100, ab34710, Abcam), type II collagen (1:100, ab34712, Abcam) and acetylated-tubulin antibody (1:100, T6793, Sigma) in blocking buffer at 4 °C overnight. Tissue sections were washed 3 times with PBS. Alexa Fluor 488-conjugated anti-rabbit (1:200, A11008, Invitrogen) and Alexa Fluor 647-conjugated anti-mouse (1:200, A-21236, Invitrogen) antibodies were used as secondary antibodies. Coverslips were mounted with Fluoroshield (F6057, Sigma-Aldrich).

To visualize cilia in cells, immunofluorescence was performed using the primary acetylated-tubulin antibody (1:500, T6793, Sigma). Briefly, cells were serum starved for 48 h, washed with PBS and fixed with 4% paraformaldehyde at room temperature. Fixed cells were permeabilized with 0.05% Triton X-100 and then incubated with the primary antibodies overnight at 4 °C. Alexa Fluor 647-conjugated anti-mouse (1:1,000, A-21236, Invitrogen) antibodies were used as secondary antibodies. Coverslips were mounted with Fluoroshield.

To quantify cilia length, multiple fields of Z-stacked pictures were randomly captured. The intensity profiles along the cilia were determined by drawing a boundary across the length of the primary cilia using free hand tool and measuring intensity within the boundary using ImageJ software. At least 200 cells in total in each compartment of each sample (40 X magnification, five sections collected in each sample) were measured. To quantify cilia percentage, multiple fields of Z-stacked pictures were randomly collected. Ciliated cell numbers were counted on each image. At least 30 images were be measured. The percentage of ciliated cell was calculated from the ratio of ciliated cells over total cells observed in each compartment and each sample (40 X magnification, five sections collected in each sample). Six mice were evaluated in each group. Assessments were independently done by two

authors who were blinded to the treatment or groups. The average cilia percentage and cilia length in each sample were pooled and calculated by two authors. The average cilia percentage and length in each group from six mice were pooled and calculated.

Micro-CT analysis

Quantitative analysis of the gross bone morphology and microarchitecture was performed by Micro-CT (Micro-CT 35, Scanco Medical AG, Brüttisellen, Switzerland) at Penn Center for Musculoskeletal Disorders (PCMD), University of Pennsylvania. Briefly, the third lumbar spine from 4-week-old $IFT80^{fl/fl}$ and Col-creERT; $IFT80^{fl/fl}$ mice were fixed, scanned and reconstituted as three-dimensional images. Cancellous bones were evaluated in the third lumbar spine. The cross-sectional scans were analyzed to quantify the changes in trabecular bone microarchitecture by analyzing an ROI that contoured the outer boundary of the trabecular bone throughout the entire third lumbar vertebral body, excluding the cortical bone. The ROIs were then compiled into 3D data sets using a Gaussian filter (sigma=1.2, support=2) to reduce noise and converted to binary images with a fixed grayscale threshold of 316. The 3D data sets were assessed for the following parameters: the percentage of bone volume (BV/TV, %), trabecular number (Tb.N, mm^{-1}), trabecular thickness (Tb.Th, mm) and trabecular spacing (Tb.Sp, mm). Five mice were evaluated in each group.

TUNEL assay

The TUNEL assay was performed on disc tissue sections using the “In situ cell death detection” Kit (TMR red, Sigma). Briefly, sections were deparaffinized and rehydrated before permeabilization with Proteinase K (20μg/mL, D3001–2-5, Zymo Research) for 15 min at room temperature. Then, the TUNEL assay was carried out following the manufacturer’s protocol. Coverslips were mounted with Fluoroshield. All sections were visualized using a Leica fluorescence microscope (DMI6000B, Leica). Three mice were evaluated in each group.

Mouse NP tissue organ culture and OAF cell culture

Briefly, the NP tissue organs were isolated from the NP region of IVDs in the spinal column from the first lumbar spine to the tenth tail region (23). The dissected NP tissues were briefly rinsed in sterile PBS and immediately placed in 6-well cell culture plates containing culture medium (10% FBS in αMEM with penicillin and streptomycin). NP tissues from $IFT80^{fl/fl}$ mice were infected with adenovirus (Ad) either Cre (Ad-CMV-Cre, #1405, Vector Biolabs) or GFP (Ad-GFP, #1060, Vector Biolabs) for 24 h as described in (12). The deletion efficiency of IFT80 was confirmed by RT-PCR analysis.

For OAF cell culture, the OAF was isolated as described previously (24). In brief, OAF tissues were digested initially with protease (53702–25KU, EMD Millipore) for 1 h with agitation on a shaker, followed by collagenase-P (11213865001, Sigma-Aldrich) for another 12 h at 37 °C. The digested cells were washed twice with PBS and cultured in DMEM (Gibco) supplemented with 10% FBS and 1% penicillin–streptomycin to 80%–90% confluence at 37 °C and 5% CO_2. OAF cells from $IFT80^{fl/fl}$ mice were infected with Adenovirus-Cre (Ad-Cre) as described previously to delete IFT80 gene, and cells infected with Adenovirus-GFP (Ad-GFP) served as a control (12).

Real-time RT-PCR analysis

Whole IVD tissues (without OAF) and the OAF were dissected respectively from lumbar and caudal discs of 4-week-old Col2-creERT; IFT80$^{fl/fl}$ and IFT80$^{fl/fl}$ mice, and immediately placed in Trizol for RNA isolation (15596018, Thermo Fisher Scientific). Additionally, Total RNA was also extracted from *in vitro* NP organ culture tissues and AF cells using Trizol reagent following the manufacturer's instructions. cDNA was synthesized from 2μg of total RNA. qPCR was performed with SYBR Green PCR master Mix (B21202, Bimake). All qPCR reactions were run in triplicate and normalized to the expression of GAPDH. The calculation of relative expression was performed according to the 2-ddCT method. Each reaction was run in triplicate and independently repeated three times. The sequences and product lengths for each primer pair are included in Table 2.

Western blot

Western blotting was performed to detect IFT80 and Col1α1 expression using the rabbit anti-IFT80 antibody (1:400, SAB2700413, Sigma) and rabbit anti-Col1α1 antibody (1:100, Abcam, ab34710) as described previously (12). Briefly, the Ad-GFP or Ad-Cre infected cells were lysed with NP 40 buffer (1% NP-40, 0.15 M NaCl, 50 mM Tris, pH 8.0) containing a protease inhibitor cocktail (PI78441, Fisher Scientific). The cell lysates were centrifuged at 12,000 g for 10 min at 4 °C, and the supernatants were stored at −80 °C. Protein concentration was measured using BCA protein assay reagent (23225, Fisher Scientific). Equal amounts of protein (approximately 20μg) were denatured in SDS containing Laemmli buffer and separated in 10% SDS–PAGE gels. Proteins were transferred to polyvinylidene difluoride membranes (Millipore) in buffer containing 25mM Tris, 192mM glycine and 20% methanol. The membranes were blocked with 5% non-fat milk, incubated with a primary antibody overnight at 4°C and then incubated with the horseradish peroxidase (HRP)-conjugated goat anti-rabbit IgG antibody (1:10,000, A-11034, Novex) at room temperature for 1 h. Enhanced chemiluminescence was performed with Western Bright ECL HRP (Biorad). β-actin (1:2,000, sc-47778, Santa Cruz) was probed as an internal control. The western blotting was repeated on three independent samples for each experimental group.

Scanning electron microscopy

Lumbar spine discs (L4/5) and caudal spine discs (C7/8) from 4-week-old IFT80$^{fl/fl}$; Col1-creERT or IFT80$^{fl/fl}$ mice were dissected and fixed in 2.5% (v/v) glutaraldehyde at 4 °C. The collagen fiber diameters were measured using SEM analysis as described previously (25). Briefly, the samples were digested in 20.4 U/ml hyaluronidase (H3506, Sigma) and 0.1 mg/ml bovine pancreatic trypsin (T1426, Sigma-Aldrich). The fixed samples were washed three times with PBS. The specimens were dehydrated in a graded ethyl alcohol (EtOH) series (30%, 50%, 70%, 80%, 90%, and 100%). Subsequently, specimens were dehydrated in ethanol and hexamethyldisilizane (HMDS) solutions, starting with EtOH: HMDS (1:1) and serially increasing to EtOH: HMDS (1:4), and finally washed with 100% HMDS. The samples were air dried in the fume hood for one hour. Samples were mounted on the AI-hold with super glue and coated with carbon. The FEI XL30 ESEM (FEI XL30 ESEM, FESEM Thermo Fisher, 5350 NE Dawson Creek Drive, Hillsboro, Oregon 97124 USA, voltage: 8

kV) was used for imaging. ImageJ software was used for the measurement of collagen fibril diameters. Six mice were evaluated in each group.

BrdU cell proliferation assay

OAF cells from IFT80$^{fl/fl}$ mice were infected with Ad-Cre (with or without SAG treatment) or Ad-GFP and cultured for 2–3 days. The cultures were incubated with BrdU solution (1:100, 000103, Invitrogen, USA) for 20 h, and stained with a BrdU staining kit (1:100, MA3071, Invitrogen, USA) according to the manufacturer's instructions. BrdU positive and total cell numbers were counted in 10 images per subject. The number of BrdU-positive cells was indicated as a percentage of the total cell number. BrdU assay was repeated on three independent samples for each experimental group.

Statistics

All data are presented as mean±s.d. Shapiro-Wilk test for the normality and Bartlett test for variance were performed to determine the appropriate statistical tests. Student's-test for the comparison between two groups or one-way ANOVA followed by Tukey's multiple comparison test for grouped samples was performed. The number of animals, and repetitions of experiments were presented in figure legends. The program GraphPad Prism (GraphPad Software, Inc., San Diego, USA) was used for these analyses. *P<0.05, **P<0.01, ***P<0.0001. NS = not statistically significant.

Results

Primary cilia are present and exhibit a significant difference in the ciliary number and length of each IVD component tissue

Primary cilia in 4-week-old CMV-cilia-GFP mice were respectively detected in 50–80%, 30–60%, 20–40% and 20–50% of cells in the GP, EP, NP and AF of the frozen IVD sections from the mouse lumbar spine (L3-L5) and tail (C7–8) (Table 1) (Fig. 1A). The cilia length ranged from 0.5–4μm in the GP and EP, 0.5–3.5μm in the AF (Fig. 1A). Notably, cilia length varied widely in the NP from 0.5μm to 15μm, (Fig. 1B), which are the longest cilia found in the mouse musculoskeletal system. Scanning electron microscopy (SEM) studies showed that the cilia in the AF typically appeared as single antenna-like strands named axoneme, projecting from the cell (Fig. 1C).

Age affects primary cilia number and length in NP

To examine whether age affects primary cilia formation in NP and AF, we first analyzed the percentage of ciliated cells and cilia length in mouse lumbar spine (L3-L5) at different ages of CMV-cilia-GFP mice (Fig. 2A). About 25.3%, 28.3%, 25.9% of NP cells in postnatal day 0 (P0), 1 month (1M), 3M-old CMV-cilia-GFP mice had cilia, however, there were only 14.1% of NP cells with cilia at 24-month-old mouse (Fig. 2A, B). The percentage of ciliated cells in AF was 38.3%, 36.2%, 38.2% and 36.8% at P0, 1M, 3M and 24M respectively (Fig. 2B). The average primary cilia length in NP was 1.32μm at P0. It increased to 3.7μm at 1M and 4.1μm at 3M but decreased to 2.7μm at 24M (Fig. 2C). The average primary cilia length in AF was 1.38μm, 1.37μm, 1.39μm at P0, 1M and 3M, but decreased to1.2μm at 24M (Fig. 2C).

IVD injury and repair impacts cilia number and orientation

To define whether IVD injury affect primary cilia numbers, we generated injury induced IVDD in mice tail IVD (Fig. 3A). By performing immunofluorescence staining for acetylated tubulin, a primary cilia marker in IVDs from the intact controls and injured mice, we found that the cilia numbers were reduced by 15.3% in NP and 24.6% in AF at 1 week following coccygeal IVD injury compared to the intact mice (Fig. 3A, C). Safranin O fast green staining results showed that the jelly-like material of NP was lost at 4w after injury (Fig. 3B). Immunofluorescence staining showed the percentage ciliated cells in AF increased by 65.6% at 4 week following injury during the IVD repair stage as compared to intact mice (Fig. 3B, D)(26). Although the cilia incidence in GP had no significant difference between intact and injured IVD at 4 weeks following injury, cell alignment and primary cilia orientation were impaired in the injured group (Fig. 3B D).

Deletion of IFT80 in type II collagen positive (Col2^{+}) cells causes an early onset of the IVDD phenotype

To study whether primary cilia and ciliary IFT80 play a role in IVD cells, IFT80$^{fl/fl}$ and IFT80$^{fl/fl}$; Col2-creERT mice were I.P. administered with TM at postnatal days 3, 5, and 7. We first confirmed the efficiency of IFT80 deletion in the IVD isolated from the IFT80$^{fl/fl}$; Col2-creERT mice (Supplement figure 1, Fig. 8A). The results from H&E and Safranin O/ fast green staining showed that the stereotypical columnar structure of the chondrocytes in the GP(27) was disrupted and that the height of EP region and the number and size of EP cells were apparently reduced in IFT80$^{fl/fl}$; Col2-creERT mice (Fig. 4A, B, C). Quantitative analysis revealed that 81.1% of GP cells in IFT80$^{fl/fl}$ controls were organized into continuous columns, but in IFT80$^{fl/fl}$; Col2-creERT mice, only 22.3% of GP cells formed continuous columns (Fig. 4D). Additionally, the columns index(28) was significantly decreased from 326.1 in IFT80$^{fl/fl}$ control group to 79.3 in IFT80 deleted group, indicating that deletion of IFT80 causes a defect in chondrocyte organization (Fig. 4D). Moreover, the cell morphology in the NP and IAF of IFT80$^{fl/fl}$; Col2-creERT mice exhibited a greater loss of alignment pattern compared with that in IFT80$^{fl/fl}$ controls (Fig. 4A, B).

IFT80 ablation in type I collagen positive (Col1^{+}) cells causes a disorganized microstructural pattern of collagen fibers in the OAF and decreased bone mass in vertebral bone

To study whether primary cilia and ciliary IFT80 play a role in OAF cells, age- matched IFT80$^{fl/fl}$; Col1-creERT mice and IFT80$^{fl/fl}$ control mice were administered with TM at postnatal days 3, 5, and 7 (Fig. 8B, Supplement figure 2). The results from H&E staining analysis of IVD showed that the OAF exhibited disorganized, loosened and disconnected fibrous rings in IFT80$^{fl/fl}$; Col1-creERT mice compared to control mice (Fig. 4E). To gain further insight into the altered fibrous structure in the OAF, we employed SEM to observe the extracellular matrix (ECM). As shown in Fig. 4F, the surface of the OAF was folded into regular and smooth ridges and grooves that ran on a wavy plane in control samples. In contrast, the plane of ridges and grooves was markedly distorted and disorganized in IFT80$^{fl/fl}$; Col1-creERT mice. Quantitative analysis revealed that the diameter of collagen fibrils in IFT80$^{fl/fl}$; Col1-creERT mice was significantly smaller than that in IFT80$^{fl/fl}$ mice,

indicating that IFT80 plays an essential role for the proper arrangement of OAF fibrous rings (Fig. 4G, H, I).

In addition a reduction in bone mass was observed in the IFT80$^{fl/fl}$; Col1-creERT vertebrae compared to that in IFT80$^{fl/fl}$ control vertebrae (Fig. 5A). In particular, BV/TV (Fig. 5B), Tb.N (Fig. 5C), and Tb.Th (Fig. 5D) were reduced to approximately 0.5-, 0.75-, and 0.6-fold, respectively, whereas Tb.Sp (Fig. 5E) was increased 1.8-fold in IFT80$^{fl/fl}$; Col1-creERT mice compared to those in IFT80$^{fl/fl}$ controls.

IFT80 ablation impairs ciliogenesis, collagen expression and cell organization in IVD

To further analyze primary cilia formation and collagen expression, we performed immunofluorescence staining for acetylated tubulin, a primary cilia marker, and Col2α1 or Col1α1 in IVDs from the IFT80$^{fl/fl}$ controls and IFT80$^{fl/fl}$; Col2-creERT mice. The results showed that the cilia numbers were reduced by approximately 0.55-, 0.52-, 0.58- and 0.37-fold in the GP, EP, IAF and NP respectively in IFT80$^{fl/fl}$; Col2-creERT mice compared to IFT80$^{fl/fl}$ mice (Fig. 6A, B). Consistently, only 13% of cells in the OAF of IFT80$^{fl/fl}$; Col1-creERT mice, whereas 31% of cells in IFT80$^{fl/fl}$ controls contained cilia (Fig. 6C, D). Moreover, compared to the IFT80$^{fl/fl}$ IVDs, deletion of IFT80 downregulated Col2α1 expression levels in the GP, EP, IAF and NP and the Col1α1 expression levels in the OAF.

Deletion of IFT80 promotes cell apoptosis in IVD cells and decreases OAF cell proliferation

To gain insight into the cellular mechanisms of IVD defects caused by IFT80 deletion, TUNEL staining was performed to detect cell apoptosis. Interestingly, we observed a remarkable increase in TUNEL-positive signaling from 5% to 33% in in the GP, EP, IAF and NP of IFT80$^{fl/fl}$; Col2-creERT mice compared to those in IFT80$^{fl/fl}$ mice (Fig. 7A, C). Similarly, increased TUNEL positive cell percentage was observed in the OAF region from less than 2% in IFT80$^{fl/fl}$ mice to 28% in IFT80$^{fl/fl}$; Col1-creERT mice, indicating that ciliary IFT80 is involved in the maintenance of cell survival (Fig. 7B, D).

To further test whether cell proliferation was affected by IFT80 deletion, we performed an *in vitro* colorimetric WST-1 cell proliferation assay in primary OAF cells isolated from IFT80$^{fl/fl}$ mice (24). Cells were treated with either Ad-GFP for controls or Ad-Cre for IFT80 deletion, and then subjected to the culture media with increasing percentages of serum. The results showed that the cell proliferation rate in IFT80 deleted cells were a 0.64-, 0.63-, 0.61-, and 0.66-fold less than those in the control cells with 1%, 2%, 5%, and 10% serum-containing media, respectively (Supplement figure 3), indicating that IFT80 is necessary for cell proliferation.

Deletion of IFT80 decreases the IVD marker gene expression and disrupts Hh signaling

To gain further insights into the mechanism by which IFT80 regulates in IVD, mouse IVDs (without the OAF) were isolated from TM-treated IFT80$^{fl/fl}$ and IFT80$^{fl/fl}$; Col2-creERT mice, and the total RNA from these samples was extracted. The expression level of IFT80 was significantly decreased in IFT80$^{fl/fl}$; Col2-creERT group, confirming efficient gene deletion (Fig. 8A). The levels of Col2α1, Col1α1, Sox9, and aggrecan in IFT80 deleted IVDs were decreased to 0.3-, 0.1-, 0.45-, and 0.7-fold than control IVDs, respectively,

indicating that ciliary IFT80 is important for the gene expression of IVD markers (Fig. 8A). Significantly increased levels of MMP3 in IVDs of IFT80$^{fl/fl}$; Col2-creERT mice indicated the existence of IVD degeneration. In addition, the expression levels of Patch1 and Gli1, the signaling components of Hh signaling, were reduced to 0.7- and 0.6-fold compared to those in the controls, suggesting that IFT80 is essential for the expression of IVD markers and Hh signal transduction (Fig. 8A). In addition, by isolating the OAF tissues from TM-treated IFT80$^{fl/fl}$ and IFT80$^{fl/fl}$; Col1-creERT mice, we found that the gene expression levels of IFT80 and Col1α1 decreased to 0.5- and 0.4-fold in IFT80$^{fl/fl}$; Col1-creERT mice compared to the levels in the controls, respectively (Fig. 8B). The levels of Patch1 and Gli1 were also reduced to 0.3- and 0.75-fold compared to the levels in the controls, suggesting that deletion of IFT80 impairs Col1α1 expression and Hh signaling in the OAF (Fig. 8B).

To further analyze the effect of IFT80 on the NP, NP tissues organs were isolated from IFT80$^{fl/fl}$ mice and subsequently infected with either Ad-GFP or Ad-Cre as described in Methods. The viral infection efficiency was tested by evaluating GFP fluorescent signals in the adenovirus-infected cells (Fig. 8C). Gene expression analysis of IFT80 confirmed the gene deletion efficiency of Ad-Cre (Fig. 8D). Col2α1, Col1α1, Sox9, and aggrecan in IFT80 deleted cells decreased to 0.2-, 0.65-, 0.6-, and 0.2-fold, than controls, indicating that IFT80 was important for the NP development and function (Fig. 8D). Similarly, the transcriptional levels of Patch1 and Gli1 in IFT80 deleted cells were reduced to 0.35- and 0.3-fold than controls. Likewise, to test the effect of IFT80 on the OAF *in vitro*, we isolated primary cells from the IFT80$^{fl/fl}$ mouse OAF tissue and infected with either Ad-GFP or Ad-Cre. Immunofluorescence staining for acetylated-tubulin showed a significance decrease in both cilia length and percentage in Ad-Cre-infected cells compared to the control (Fig. 8E, F). Western blot analysis confirmed a significant decrease in IFT80 and Col1α1expression in Ad-cre-infected cells (Fig. 8G, H, I), suggesting that deletion of IFT80 down regulates the gene expression of Col1α1. Furthermore, the gene expression of Patch1 and Gli1 was reduced to 0.25- and 0.4-fold, respectively (Fig. 8G). These findings demonstrate that ciliary IFT80 regulates Col1α1 expression and Hh signaling in the OAF cells.

Smoothened agonist (SAG) rescued deficient OAF cell proliferation and differentiation in IFT80 silenced cells

To further test whether IFT80 deletion caused defective OAF cell proliferation and differentiation can be rescued by Hh/Smo agonist, we isolated primary OAF cells from the IFT80$^{fl/fl}$ mouse OAF tissue. Cells at passage 1 were infected with either Ad-GFP or Ad-Cre and treated with SAG. BrdU staining showed that deletion of IFT80 reduced OAF cell proliferation, which can be partially rescued by SAG treatment (Figure 8J, K). It was reported AF cell have the osteogenic potential (29). To study whether IFT80 deletion can impair osteogenic differentiation ability of OAF cell and whether this defect can be rescue by SAG treatment, we treated Ad-GFP and Ad-Cre infected OAF cells with SAG and induced cell differentiation with osteogenic media for 21 day. The results showed that deletion of IFT80 significantly inhibited OAF cell osteogenic differentiation, and SAG treatment promoted the osteogenic differentiation in both the control and IFT80 deficient cells (Figure 8L, M). Consistently, the treatment with SAG significantly increased gene

expression levels of Col1α1, Patch1 and Gli1 in IFT80 deficient group compared to the untreated IFT80 deficient group (Fig. 8N).

Discussion

Previous studies (30, 31) reported that cilia are present in rat AF tissues and in *in vitro* cultured mouse and human NP cells; however, the distribution and arrangement of cilia in IVD components *in vivo* is still unknown. In this study, we reveal for the first time that primary cilia are present in mouse IVD *in vivo*. We found that cilia length in the GP and EP were 0.5–4μm, similar to the ones reported in chondrocytes(32). The cilia length in AF is relatively shorter than those in the GP and EP and varied from 0.5 to 3.5μm. Most interestingly, the cilia length in the mouse NP was largely variable, with some cilia were as short as 0.5μm and some up to 15μm. The varied ciliary lengths in NP cells might be due to the mixed cell types (33, 34) and/or the dynamic assembly and disassembly of cilia in NP unique mechanical and jelly like matrix environment. Although the requisition of long cilia in the NP is unclear yet, some studies suggest that the longer cilium has unique function. For example, olfactory cilia are 50–60μm in length, representing the longest cilia so far found in human (35). The kinocilium, 10–15μm in length, serves to polarize the actin-based stereocilia during development of auditory hair cells (36). In general, a longer cilium increases the torque, which is the cross product of the lever-arm vector and the force vector, leading to a renewed force equilibrium(32). As suggested by Resnick et al.(37), the longer the cilium, the more sensitive the cells response to the flow changes, because less force is needed to bend the cilium and activate Ca^{2+} influx. The NP is full of a highly hydrated jelly like materials, and it allows the movement of the spine by deforming and altering the shape of the IVD under compression, tilting, and twisting conditions(38). The longer cilia in the NP may make the cells more sensitive to sense the mechanical and chemical signals and direct cells to move around and respond to environment as the force changes in the IVDs.

Advancing age is the greatest risk factor for spine-related chronic disability and back pain, which stems from age-associated IVDD (39). Primary cilia and aging have been investigated by several studies. Cornils et al.(40) reported the increased variability in ASI cilia length as animal aged. Recently, it was reported that primary cilia length are frequently changed in aging related and neurodegenerative disorders(41). However, it is unknown whether cilia are involved in aged and/or injury induced IVDD. We found for the first time that primary cilia length and percentage significantly decreased in NP at 24-month old compared to 3-month old. Moreover, we found that the percentage of ciliated cells were dramatically decreased in NP and AF at 1 week following IVD injury. These findings suggest that injury or mechanical stimulation can alter cilia formation. Interestingly, at 4 weeks following injury, which is the stage of AF repair (26), cilia number in AF of IVD injured mice significantly increased compared with that in the intact mice, indicating primary cilia are important for the IVD repair and regeneration. Thus, promoting ciliogenesis in AF and NP could be a potential target for the treatment of IVDD in the future.

TM inducible Col2-creERT (42) and Col1-creERT (43) mice have been shown to express Cre specifically in the IAF, GP, EP and NP, and OAF of the IVD respectively. To further determine whether primary cilia involve in IVD development, maintenance and

degeneration, we deleted IFT80 in mouse IVD by using Col2-creERT and Col1-creERT mice respectively. As we expected, deletion of IFT80 exhibited evident IVDD phenotype. Cilia numbers were markedly decreased in $Col2^{+}$ regions including GP, EP, IAF and NP, and $Col1^{+}$ region in OAF. Besides these, $IFT80^{fl/fl}$; Col2-creERT mice displayed disrupted IVD structure with disorganized and decreased GP and EP formation. This is supported by our previous findings that deletion of IFT80 in $Col2^{+}$ cells severely disrupted GP development and cartilage formation in long bone (12, 18). Although lineage tracing $Col2^{+}$ cells with tomato mice in IVD showed very limited tdtomato positive signaling in NP(42), the evident phenotype and specific staining of more apoptotic cells shown in the NP suggested that the NP cells could be affected through an indirect effect or cell-to-cell communication. Further investigation needs to be done in the future.

For the first time, we found that cilia loss induced by IFT80 deletion causes cell apoptosis in IVD cells, including chondrocytes, suggesting that primary cilia are critical for the regulation of cell apoptosis, and cell loss is an important contributor to the defective phenotype in IFT80-deleted IVD, such as the decreased cell number in the EP, the reduction of ECM in the NP and AF, and the loss of trabecular bone. This is also supported by the observation from Wang et al (44), where they report that cilia loss induced cell apoptosis in tubular epithelial cell. Additionally, Brian et al.(45) also proved that the stabilization of neuronal primary cilia can inhibit apoptotic cell cycling.

The intimate relationship between cilia and extracellular matrix (ECM) has been reported in many tissues and organs (11, 46). ECM receptor is detected on primary cilia in chondrocyte (11). Fibrosis and abnormal ECM are observed in ciliopathies such as autosomal dominant polycystic kidney disease, nephronophthisis, and Bardet-Biedl syndrome (46). Interestingly, our findings showed that ablation of cilia by IFT80 deletion can reduce collagen formation and organization in each part of IVD, especially in AF. SEM results showed the dramatically disorganized collagen assembly in OAF. These data suggested that cilia and IFT80 are required for fiber orientation and arrangement in AF. Similar to the arrangement of plies in a modern automobile tire, the well organization of collagen fibers and laminae in the AF allows the anulus to contain hydrostatic pressure loads (47). Moreover, the AF is also able to provide resistance to minor displacements of the adjacent vertebral bodies because of the variation in fiber orientation. However, the disorganized fiber patterns caused by the loss of cilia disrupt the normal function of AF. Besides these, our results showed that the Col1α1 and Col2α1 levels dramatically decreased, in contrast, MMP3 levels increased in IVD after ablation of cilia by IFT80 deletion. These results are supported by previous findings that ciliary IFT20 regulates collagen production and intracellular trafficking in the multipotent stem cells of cranial neural crests (48) and that ciliary IFT88 deletion in articular cartilage enhances the expression of MMP13 to degrade the collagen (10).

Notably, deletion of IFT80 caused the phenotype of shortened GP and EP and loosened NP is very similar to the IVD phenotype in India hedgehog (Ihh) knock out mice ($Ihh^{fl/fl}$; Col2-creERT) (49), suggesting that IFT80 regulates IVD likely through Hh signaling pathway. Indeed, we found that deletion of IFT80 down regulates Patch1 and Gli1 expression. Moreover, Hh/Smoothen agonist-SAG treatment can significantly increase OAF cell proliferation, differentiation, collagen and Patch and Gli1expression. In agreement with our

observations, sonic hedgehog signaling has been proven to increase cell viability and inhibit cell apoptosis by upregulating the expression of Patch1, and Gli1 in HCT116 myofibroblastic cell and IVD cells (44, 50, 51). These findings demonstrate that deletion of IFT80 in IVD causes cilia loss, which impairs Hh signaling transduction and eventually causes cell apoptosis and defects in cell differentiation and proliferation in IVDs.

In summary, our study for the first time, reveal that primary cilia are present in each compartment of the IVD and aging and injury in IVD affects primary cilia formation. Moreover, ciliary IFT80 is important for the maintenance of IVD cells and collagen organization, cell survival and proliferation via regulating Hh signaling. Thus, our findings may provide new insights into the etiologies and pathology for IVDD and related diseases. However, considering the different mechanical force and anatomy of IVD between mice and human (52, 53), further study of primary cilia in human IVD are needed in the future.

Supplementary Material

Refer to Web version on PubMed Central for supplementary material.

Acknowledgements

Research reported in this publication was supported by the National Institute of Dental and Craniofacial Research and the National Institute of Arthritis and Musculoskeletal and Skin Diseases, and National Institute on Aging, part of the National Institutes of Health, under Award Numbers DE023105, AR066101 and AG048388 to S.Y. XL was supported by China Scholarship Council (CSC) Grant #201706260178. The content is solely the responsibility of the authors and does not necessarily represent the official views of the National Institutes of Health.

The authors acknowledge Penn Center for Musculoskeletal Disorders for providing access to the microCT instrument (NIH/NIAMS P30 AR069619). The authors acknowledge technical support and suggestion provided by Yejia Zhang, Zuozhen Tian and Jormay Lim at the University of Pennsylvania. We also thanks Dr. Vishwa Deepak for proof reading the manuscript.

ABBREVIATIONS

AF	annulus fibrosus
Ad-GFP	Adenovirus-GFP
Ad-Cre	Adenovirus-Cre
Co	coccygeal
EP	cartilage endplate
ECM	extracellular matrix
GP	growth plate
HMDS	hexamethyldisilizane
Hh	hedgehog
IAF	internal AF
Ihh	India hedgehog

IFT	Intraflagellar transport
IVD	intervertebral disc
IVDD	intervertebral disc degeneration
NP	nucleus pulposus
OAF	outer AF
SAG	Smoothened agonist
SEM	Scanning electron microscopy
TM	tamoxifen

References

1. Moriguchi Y, Alimi M, Khair T, Manolarakis G, Berlin C, Bonassar LJ, and Hartl R (2016) Biological Treatment Approaches for Degenerative Disk Disease: A Literature Review of In Vivo Animal and Clinical Data. Global Spine J 6, 497–518 [PubMed: 27433434]
2. Boos N, Weissbach S, Rohrbach H, Weiler C, Spratt KF, and Nerlich AG (2002) Classification of age-related changes in lumbar intervertebral discs: 2002 Volvo Award in basic science. Spine (Phila Pa 1976) 27, 2631–2644 [PubMed: 12461389]
3. Miller JA, Schmatz C, and Schultz AB (1988) Lumbar disc degeneration: correlation with age, sex, and spine level in 600 autopsy specimens. Spine (Phila Pa 1976) 13, 173–178 [PubMed: 3406837]
4. Raj PP (2008) Intervertebral disc: anatomy-physiology-pathophysiology-treatment. Pain Pract 8, 18–44 [PubMed: 18211591]
5. Li X, Han Y, Di Z, Cui J, Pan J, Yang M, Sun G, Tan J, and Li L (2016) Percutaneous endoscopic lumbar discectomy for lumbar disc herniation. J Clin Neurosci 33, 19–27 [PubMed: 27475315]
6. Li X, Hu Z, Cui J, Han Y, Pan J, Yang M, Tan J, Sun G, and Li L (2016) Percutaneous endoscopic lumbar discectomy for recurrent lumbar disc herniation. Int J Surg 27, 8–16 [PubMed: 26805569]
7. Adams MA, and Roughley PJ (2006) What is intervertebral disc degeneration, and what causes it? Spine (Phila Pa 1976) 31, 2151–2161 [PubMed: 16915105]
8. Beales PL, Bland E, Tobin JL, Bacchelli C, Tuysuz B, Hill J, Rix S, Pearson CG, Kai M, Hartley J, Johnson C, Irving M, Elcioglu N, Winey M, Tada M, and Scambler PJ (2007) IFT80, which encodes a conserved intraflagellar transport protein, is mutated in Jeune asphyxiating thoracic dystrophy. Nat Genet 39, 727–729 [PubMed: 17468754]
9. Goetz SC, and Anderson KV (2010) The primary cilium: a signalling centre during vertebrate development. Nat Rev Genet 11, 331–344 [PubMed: 20395968]
10. Chang CF, Ramaswamy G, and Serra R (2012) Depletion of primary cilia in articular chondrocytes results in reduced Gli3 repressor to activator ratio, increased Hedgehog signaling, and symptoms of early osteoarthritis. Osteoarthritis Cartilage 20, 152–161 [PubMed: 22173325]
11. Ruhlen R, and Marberry K (2014) The chondrocyte primary cilium. Osteoarthritis Cartilage 22, 1071–1076 [PubMed: 24879961]
12. Yuan X, Cao J, He X, Serra R, Qu J, Cao X, and Yang S (2016) Ciliary IFT80 balances canonical versus non-canonical hedgehog signalling for osteoblast differentiation. Nat Commun 7, 11024 [PubMed: 26996322]
13. Grimes DT, Boswell CW, Morante NF, Henkelman RM, Burdine RD, and Ciruna B (2016) Zebrafish models of idiopathic scoliosis link cerebrospinal fluid flow defects to spine curvature. Science 352, 1341–1344 [PubMed: 27284198]
14. Chang CF, and Serra R (2013) Ift88 regulates Hedgehog signaling, Sfrp5 expression, and beta-catenin activity in post-natal growth plate. J Orthop Res 31, 350–356 [PubMed: 23034798]

15. Thorpe SD, Gambassi S, Thompson CL, Chandrakumar C, Santucci A, and Knight MM (2017) Reduced primary cilia length and altered Arl13b expression are associated with deregulated chondrocyte Hedgehog signaling in alkaptonuria. J Cell Physiol 232, 2407–2417 [PubMed: 28158906]
16. Gambassi S, Geminiani M, Thorpe SD, Bernardini G, Millucci L, Braconi D, Orlandini M, Thompson CL, Petricci E, Manetti F, Taddei M, Knight MM, and Santucci A (2017) Smoothened-antagonists reverse homogentisic acid-induced alterations of Hedgehog signaling and primary cilium length in alkaptonuria. J Cell Physiol 232, 3103–3111 [PubMed: 28019670]
17. Wang C, Yuan X, and Yang S (2013) IFT80 is essential for chondrocyte differentiation by regulating Hedgehog and Wnt signaling pathways. Exp Cell Res 319, 623–632 [PubMed: 23333501]
18. Yuan X, and Yang S (2015) Deletion of IFT80 Impairs Epiphyseal and Articular Cartilage Formation Due to Disruption of Chondrocyte Differentiation. PLoS One 10, e0130618 [PubMed: 26098911]
19. Ballarin-Gonzalez B, Lassen LB, Jessen R, Fuchtbauer A, Fuchtbauer EM, and Pedersen FS (2013) Deregulated Nras expression in knock-in animals harboring a gammaretroviral long terminal repeat at the Nras/Csde1 locus. PLoS One 8, e56029 [PubMed: 23418499]
20. Nakamura E, Nguyen MT, and Mackem S (2006) Kinetics of tamoxifen-regulated Cre activity in mice using a cartilage-specific CreER(T) to assay temporal activity windows along the proximodistal limb skeleton. Dev Dyn 235, 2603–2612 [PubMed: 16894608]
21. Ponticos M, Abraham D, Alexakis C, Lu QL, Black C, Partridge T, and Bou-Gharios G (2004) Col1a2 enhancer regulates collagen activity during development and in adult tissue repair. Matrix Biol 22, 619–628 [PubMed: 15062855]
22. Tian Z, Ma X, Yasen M, Mauck RL, Qin L, Shofer FS, Smith LJ, Pacifici M, Enomoto-Iwamoto M, and Zhang Y (2018) Intervertebral Disc Degeneration in a Percutaneous Mouse Tail Injury Model. Am J Phys Med Rehabil 97, 170–177 [PubMed: 28863006]
23. Zhang Y, Tian Z, Ashley JW, Wang L, Tower RJ, Wei Y, Qin L, Yang S, and Enomoto-Iwamoto M (2019) Extracellular Matrix and Adhesion Molecule Gene Expression in the Normal and Injured Murine Intervertebral Disc. Am J Phys Med Rehabil 98, 35–42 [PubMed: 30085932]
24. Nakamichi R, Ito Y, Inui M, Onizuka N, Kayama T, Kataoka K, Suzuki H, Mori M, Inagawa M, Ichinose S, Lotz MK, Sakai D, Masuda K, Ozaki T, and Asahara H (2016) Mohawk promotes the maintenance and regeneration of the outer annulus fibrosus of intervertebral discs. Nat Commun 7, 12503 [PubMed: 27527664]
25. Li Q, Qu F, Han B, Wang C, Li H, Mauck RL, and Han L (2017) Micromechanical anisotropy and heterogeneity of the meniscus extracellular matrix. Acta Biomater 54, 356–366 [PubMed: 28242455]
26. Torre OM, Das R, Berenblum RE, Huang AH, and Iatridis JC (2018) Neonatal mouse intervertebral discs heal with restored function following herniation injury. FASEB J 32, 4753–4762 [PubMed: 29570392]
27. Li Y, Li A, Junge J, and Bronner M (2017) Planar cell polarity signaling coordinates oriented cell division and cell rearrangement in clonally expanding growth plate cartilage. Elife 6
28. Killion CH, Mitchell EH, Duke CG, and Serra R (2017) Mechanical loading regulates organization of the actin cytoskeleton and column formation in postnatal growth plate. Mol Biol Cell 28, 1862–1870 [PubMed: 28539407]
29. Liu C, Guo Q, Li J, Wang S, Wang Y, Li B, and Yang H (2014) Identification of rabbit annulus fibrosus-derived stem cells. PLoS One 9, e108239 [PubMed: 25259600]
30. Donnelly E, Williams R, and Farnum C (2008) The primary cilium of connective tissue cells: imaging by multiphoton microscopy. Anat Rec (Hoboken) 291, 1062–1073 [PubMed: 18727071]
31. Zheng L, Cao Y, Ni S, Qi H, Ling Z, Xu X, Zou X, Wu T, Deng R, Hu B, Gao B, Chen H, Li Y, Zhu J, Tintani F, Demehri S, Jain A, Kebaish KM, Liao S, Seguin CA, Crane JL, Wan M, Lu H, Sponseller PD, Riley LH 3rd, Zhou X, Hu J, and Cao X (2018) Ciliary parathyroid hormone signaling activates transforming growth factor-beta to maintain intervertebral disc homeostasis during aging. Bone Res 6, 21 [PubMed: 30038820]

32. Dummer A, Poelma C, DeRuiter MC, Goumans MJ, and Hierck BP (2016) Measuring the primary cilium length: improved method for unbiased high-throughput analysis. Cilia 5, 7 [PubMed: 26870322]
33. McCann MR, and Seguin CA (2016) Notochord Cells in Intervertebral Disc Development and Degeneration. J Dev Biol 4
34. Risbud MV, and Shapiro IM (2011) Notochordal cells in the adult intervertebral disc: new perspective on an old question. Crit Rev Eukaryot Gene Expr 21, 29–41 [PubMed: 21967331]
35. Challis RC, Tian H, Wang J, He J, Jiang J, Chen X, Yin W, Connelly T, Ma L, Yu CR, Pluznick JL, Storm DR, Huang L, Zhao K, and Ma M (2015) An Olfactory Cilia Pattern in the Mammalian Nose Ensures High Sensitivity to Odors. Curr Biol 25, 2503–2512 [PubMed: 26365258]
36. Choksi SP, Lauter G, Swoboda P, and Roy S (2014) Switching on cilia: transcriptional networks regulating ciliogenesis. Development 141, 1427–1441 [PubMed: 24644260]
37. Resnick A, and Hopfer U (2007) Force-response considerations in ciliary mechanosensation. Biophys J 93, 1380–1390 [PubMed: 17526573]
38. White TL, and Malone TR (1990) Effects of running on intervertebral disc height. J Orthop Sports Phys Ther 12, 139–146 [PubMed: 18796880]
39. Vo NV, Hartman RA, Patil PR, Risbud MV, Kletsas D, Iatridis JC, Hoyland JA, Le Maitre CL, Sowa GA, and Kang JD (2016) Molecular mechanisms of biological aging in intervertebral discs. J Orthop Res 34, 1289–1306 [PubMed: 26890203]
40. Cornils A, Maurya AK, Tereshko L, Kennedy J, Brear AG, Prahlad V, Blacque OE, and Sengupta P (2016) Structural and Functional Recovery of Sensory Cilia in C. elegans IFT Mutants upon Aging. PLoS Genet 12, e1006325 [PubMed: 27906968]
41. Alvarez-Satta M, Moreno-Cugnon L, and Matheu A (2019) Primary cilium and brain aging: role in neural stem cells, neurodegenerative diseases and glioblastoma. Ageing Res Rev 52, 53–63 [PubMed: 31004829]
42. Tong W, Lu Z, Qin L, Mauck RL, Smith HE, Smith LJ, Malhotra NR, Heyworth MF, Caldera F, Enomoto-Iwamoto M, and Zhang Y (2017) Cell therapy for the degenerating intervertebral disc. Transl Res 181, 49–58 [PubMed: 27986604]
43. Bedore J, Quesnel K, Quinonez D, Seguin CA, and Leask A (2016) Targeting the annulus fibrosus of the intervertebral disc: Col1a2-Cre(ER)T mice show specific activity of Cre recombinase in the outer annulus fibrosus. J Cell Commun Signal 10, 137–142 [PubMed: 27173473]
44. Wang S, Wei Q, Dong G, and Dong Z (2013) ERK-mediated suppression of cilia in cisplatin-induced tubular cell apoptosis and acute kidney injury. Biochim Biophys Acta 1832, 1582–1590 [PubMed: 23727409]
45. Choi BKA, D'Onofrio PM, Shabanzadeh AP, and Koeberle PD (2019) Stabilization of primary cilia reduces abortive cell cycle re-entry to protect injured adult CNS neurons from apoptosis. PLoS One 14, e0220056 [PubMed: 31369591]
46. Seeger-Nukpezah T, and Golemis EA (2012) The extracellular matrix and ciliary signaling. Curr Opin Cell Biol 24, 652–661 [PubMed: 22819513]
47. Vergroesen PP, Kingma I, Emanuel KS, Hoogendoorn RJ, Welting TJ, van Royen BJ, van Dieen JH, and Smit TH (2015) Mechanics and biology in intervertebral disc degeneration: a vicious circle. Osteoarthritis Cartilage 23, 1057–1070 [PubMed: 25827971]
48. Noda K, Kitami M, Kitami K, Kaku M, and Komatsu Y (2016) Canonical and noncanonical intraflagellar transport regulates craniofacial skeletal development. Proc Natl Acad Sci U S A 113, E2589–2597 [PubMed: 27118846]
49. Maeda Y, Nakamura E, Nguyen MT, Suva LJ, Swain FL, Razzaque MS, Mackem S, and Lanske B (2007) Indian Hedgehog produced by postnatal chondrocytes is essential for maintaining a growth plate and trabecular bone. Proc Natl Acad Sci U S A 104, 6382–6387 [PubMed: 17409191]
50. Shen X, Peng Y, and Li H (2017) The Injury-Related Activation of Hedgehog Signaling Pathway Modulates the Repair-Associated Inflammation in Liver Fibrosis. Front Immunol 8, 1450 [PubMed: 29163520]
51. Rajesh D, and Dahia CL (2018) Role of Sonic Hedgehog Signaling Pathway in Intervertebral Disc Formation and Maintenance. Curr Mol Biol Rep 4, 173–179 [PubMed: 30687592]

52. Daly C, Ghosh P, Jenkin G, Oehme D, and Goldschlager T (2016) A Review of Animal Models of Intervertebral Disc Degeneration: Pathophysiology, Regeneration, and Translation to the Clinic. Biomed Res Int 2016, 5952165 [PubMed: 27314030]

53. Alini M, Eisenstein SM, Ito K, Little C, Kettler AA, Masuda K, Melrose J, Ralphs J, Stokes I, and Wilke HJ (2008) Are animal models useful for studying human disc disorders/degeneration? Eur Spine J 17, 2–19 [PubMed: 17632738]

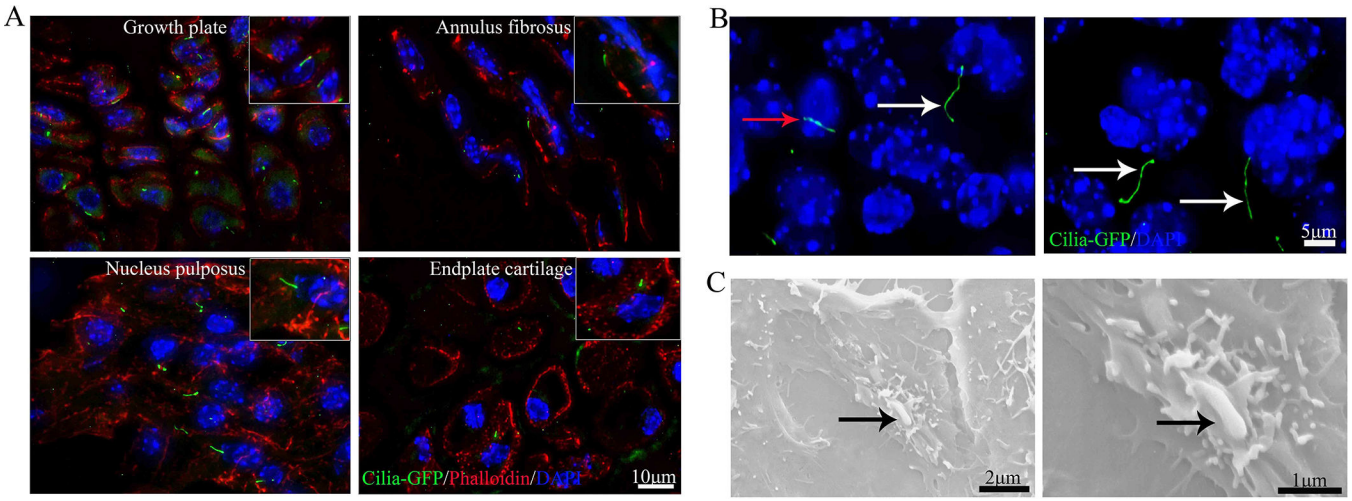

Figure 1.

Primary cilia are detected in each compartment of the IVD.

(A) Fluorescent images of coronal sections of 4-week-old CMV-Cilia-GFP mouse lumbar IVD sections. Note that primary cilia were detected in each compartment of the IVD. Green: Cilia-GFP. Red: phalloidin. Blue: DAPI. (B) Fluorescent images of 4-week-old CMV-Cilia-GFP mouse NP tissues showing different lengths of primary cilia. White arrows indicate longer cilia. Red arrows indicate shorter cilia. Green: Cilia-GFP. Blue: DAPI. (C) SEM images of the primary cilia in AF cells. Black arrow: the cilia axon. Six mice evaluated in each group.

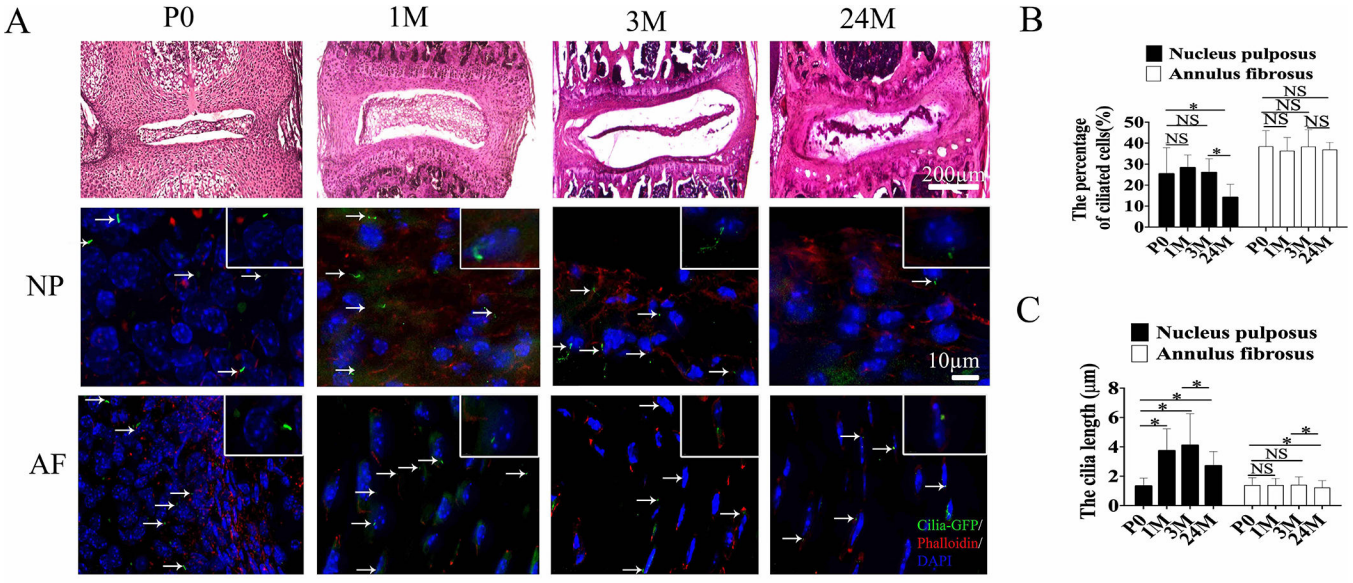

Figure 2.

Primary cilia incidence and length reduced in NP during aging induced IVDD

(A) H&E staining and fluorescent images of coronal sections of CMV-Cilia-GFP mouse lumbar IVD sections. Note that age affects primary cilia number in NP and primary cilia length in NP and AF. Green: Cilia-GFP. Red: phalloidin. Blue: DAPI. (B, C) Quantitative measurements of the percentage of ciliated cells and cilia length to the total cells per view of (A) (n=6 mice per group). All data are reported as the mean ± s.d. Statistical significance was determined by one-way ANOVA. *P<0.05, **P<0.01, ***P<0.0001. NS = not statistically significant.

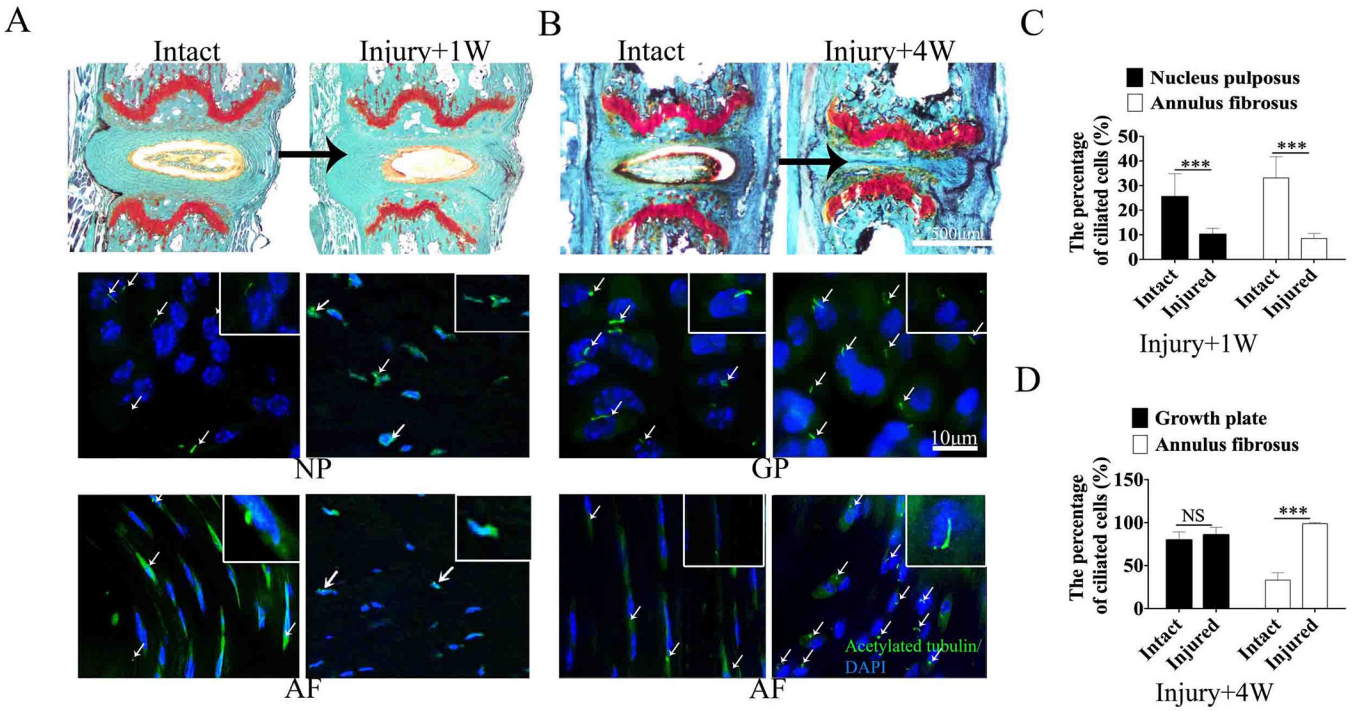

Figure 3.

IVD injury and repair impact cilia number and orientation in IVD

(A) Safranin O fast green staining and immunofluorescence staining for acetylated tubulin and DAPI of mouse lumbar IVD from intact and 1 week after coccygeal IVD injury mice. Green: Acetylated tubulin and Blue: DAPI. (B) Safranin O fast green staining and immunofluorescence staining for acetylated tubulin and DAPI of mouse lumbar IVD from intact and 4 weeks following coccygeal IVD injury. (C) Quantitative measurements of the percentage of the cells with primary cilia to the total cells per view of (A) (n=6 mice per group). (D) Quantitative measurements of the percentage of the cells with primary cilia to the total cells per view of (B) (n=6 mice per group). All data are reported as the mean ± s.d. Statistical significance was determined by Student's t-test. *P<0.05, **P<0.01, ***P<0.0001. NS = not statistically significant.

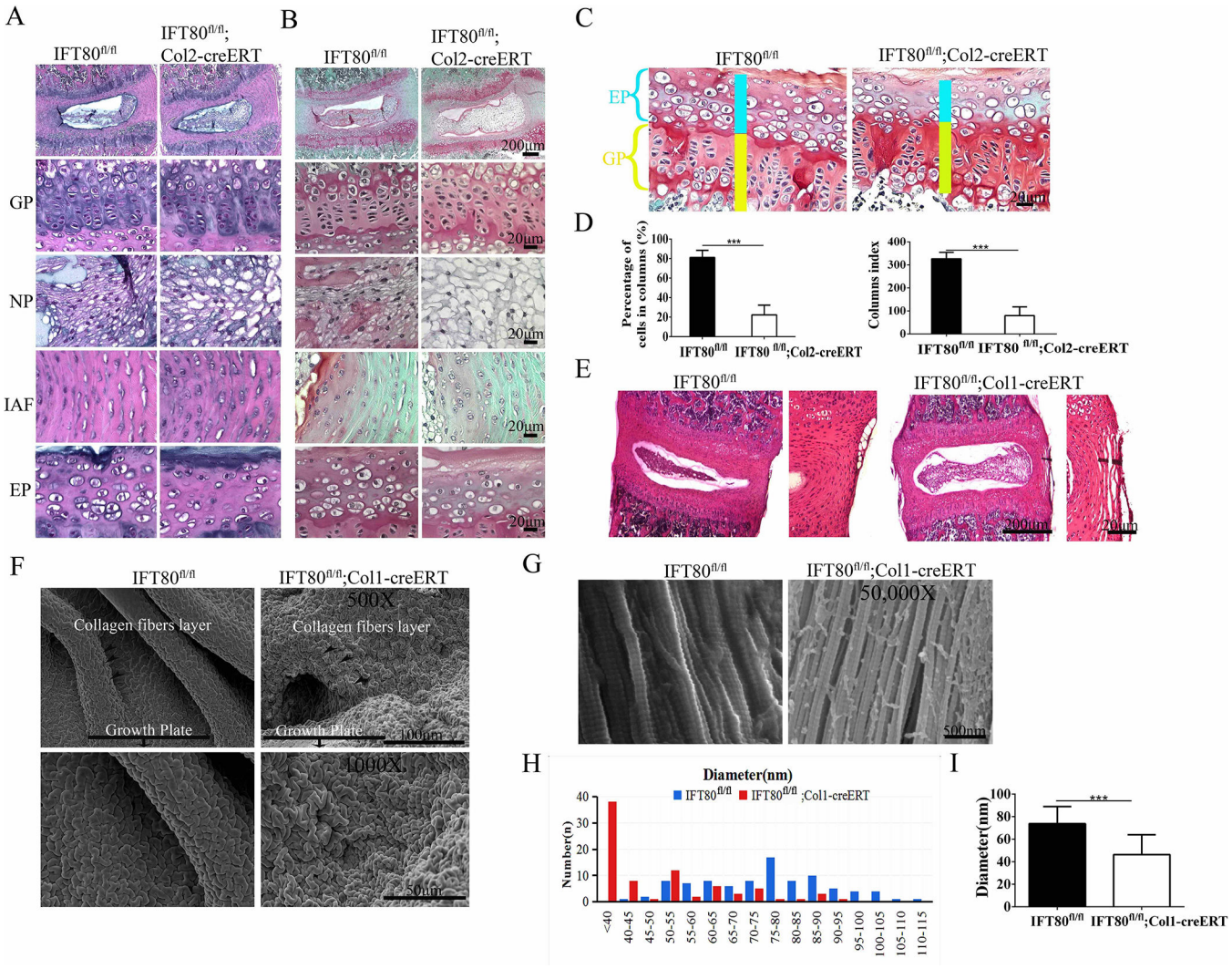

Figure 4.

Deletion of IFT80 in the IVD causes abnormal cell organization and polarity.

(A, B) H&E staining and Safranin O/fast green staining of coronal sections of IVD each compartment in 4-week-old IFT80$^{fl/fl}$ and IFT80$^{fl/fl}$; Col2-creERT mice. (C) Quantitative analysis of EP height of (B), in IFT80$^{fl/fl}$; Col2-creERT mice, the EP height was shorter, and cell size was smaller. (D) Quantitative analysis of column formation in the GP of (B) (n=6 mice per group). (E) H&E staining of coronal sections of 4-week-old IFT80$^{fl/fl}$ and IFT80$^{fl/fl}$; Col1-creERT mouse lumbar IVDs. (F) SEM images of the surface OAF of 4-week-old IFT80$^{fl/fl}$ and IFT80$^{fl/fl}$; Col1-creERT mice, black arrow: collagen fibers layer, black line with arrow: point to growth plate side. (G) High-magnification (50,000X) comparison of OAF tissue showing collagen fibers in the AF in IFT80$^{fl/fl}$ and IFT80$^{fl/fl}$; Col1-creERT mice. (H) Histogram of the diameter of collagen fibrils from 4-week-old IFT80$^{fl/fl}$ and IFT80$^{fl/fl}$; Col1-creERT mice. (I) The randomly calculated mean diameter of collagen fibrils from IFT80$^{fl/fl}$ and IFT80$^{fl/fl}$; Col1-creERT mice (n=6 mice per group). All data are reported as the mean ± s.d. Statistical significance was determined by Student's t-test. *P<0.05, **P<0.01, ***P<0.0001. NS = not statistically significant.

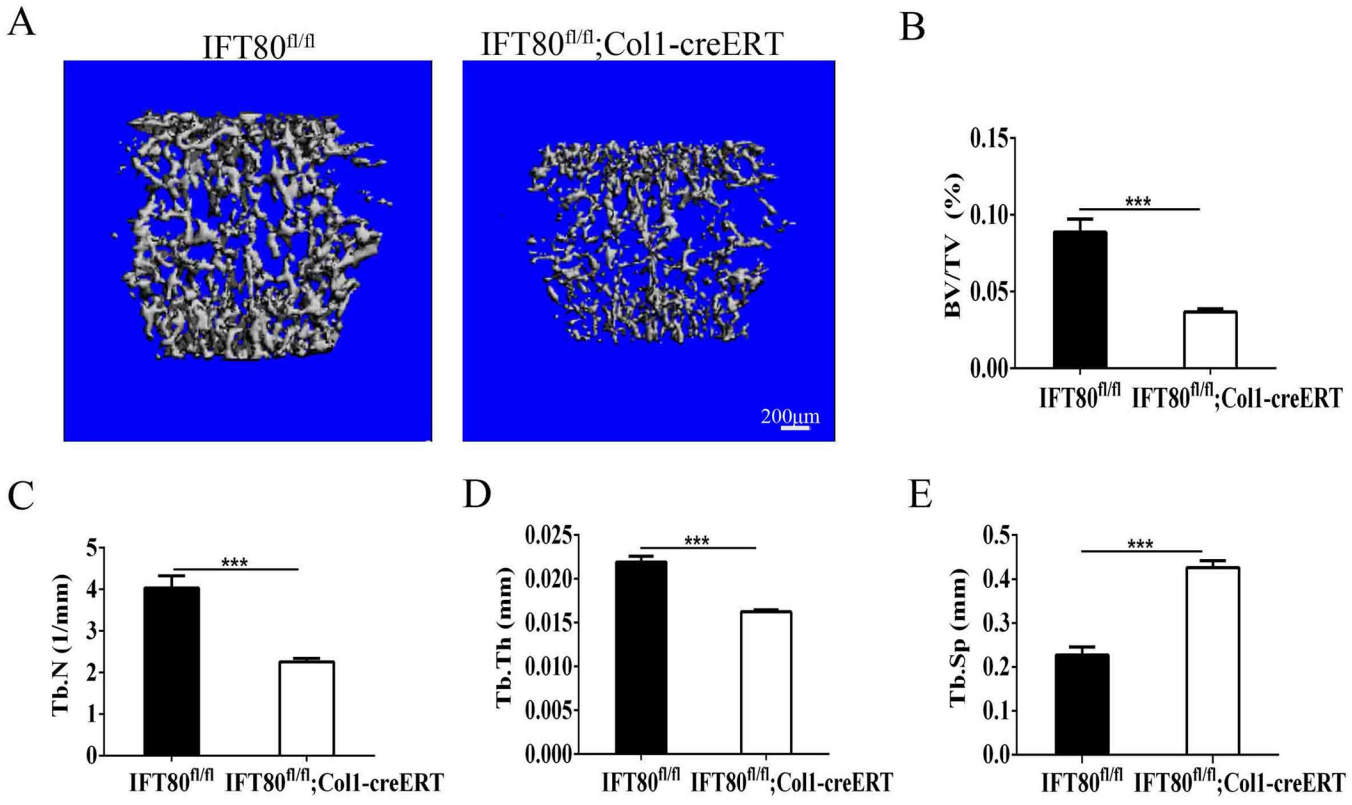

Figure 5.

Deletion of IFT80 in type I collagen-positive cells decreases bone mass in vertebral bone. (A) Representative μCT scans of the third lumbar spine of IFT80$^{fl/fl}$ and IFT80$^{fl/fl}$; Col1-creERT from 4-week old mice showing the 3D reconstructed trabecular bones. (B) Quantitative analysis of the percentage of bone volume (BV/TV). (C) Quantitative analysis of trabecular number (Tb.N). (D) Quantitative analysis of trabecular thickness (Tb.Th). (E) Quantitative analysis of trabecular spacing (Tb.Sp). All data are reported as the mean ± s.d. Statistical significance was determined by Student's t-test. NS = not significant. Five mice evaluated in each group. *P<0.05, **P<0.01, ***P<0.0001. NS = not statistically significant.

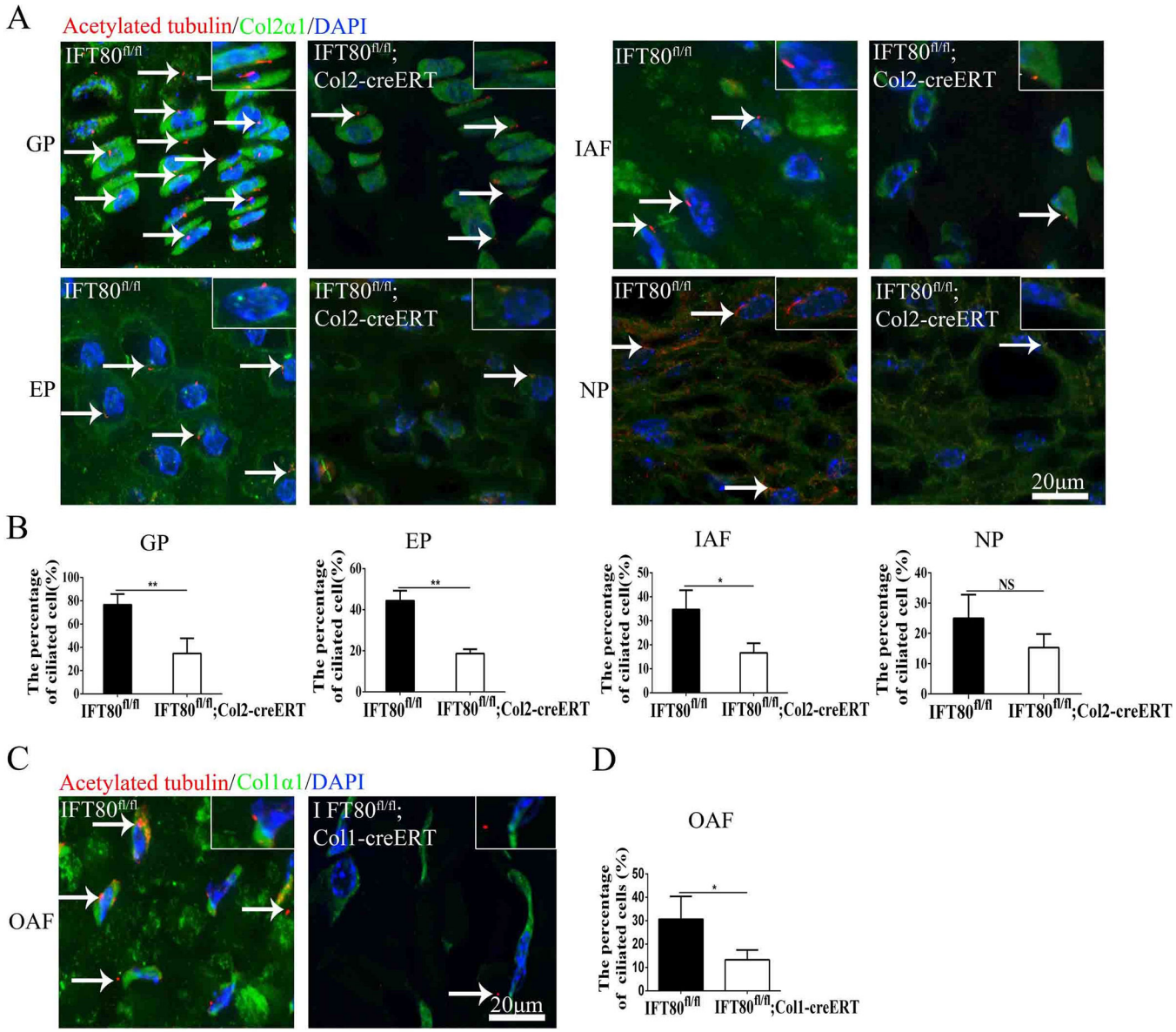

Figure 6.

IFT80 ablation impairs cillogenesis and decreases collagen expression in the mouse IVD. (A) Immunofluorescence staining for acetylated tubulin, Col2α1 and DAPI showing the length of primary cilia and Col2α1 expression in the GP, EP, IAF and NP from IFT80$^{fl/fl}$ and IFT80$^{fl/fl}$; Col2-creERT mice. Red: Acetylated tubulin, Green: Col2α1 and Blue: DAPI. (B) Quantitative measurements of the percentage of the cells with primary cilia to the total cells per view of (A) (n=6 mice per group). (C) Immunofluorescence staining for acetylated tubulin, Col1α1 and DAPI showing the primary cilia and Col1α1 expression of the outer AF (OAF) from IFT80$^{fl/fl}$ and IFT80$^{fl/fl}$; Col1-creERT mice. Red: Acetylated tubulin, Green: Col1α1 and Blue: DAPI. (D) Quantitative measurements of the percentage of the cells with primary cilia to the total cells per view (C) (n=6 mice per group). White arrow: cilia were detected by acetylated tubulin antibody. All data are reported as the mean ± s.d. Statistical

significance was determined by Student's t-test. *P<0.05, **P<0.01, ***P<0.0001. NS = not statistically significant.

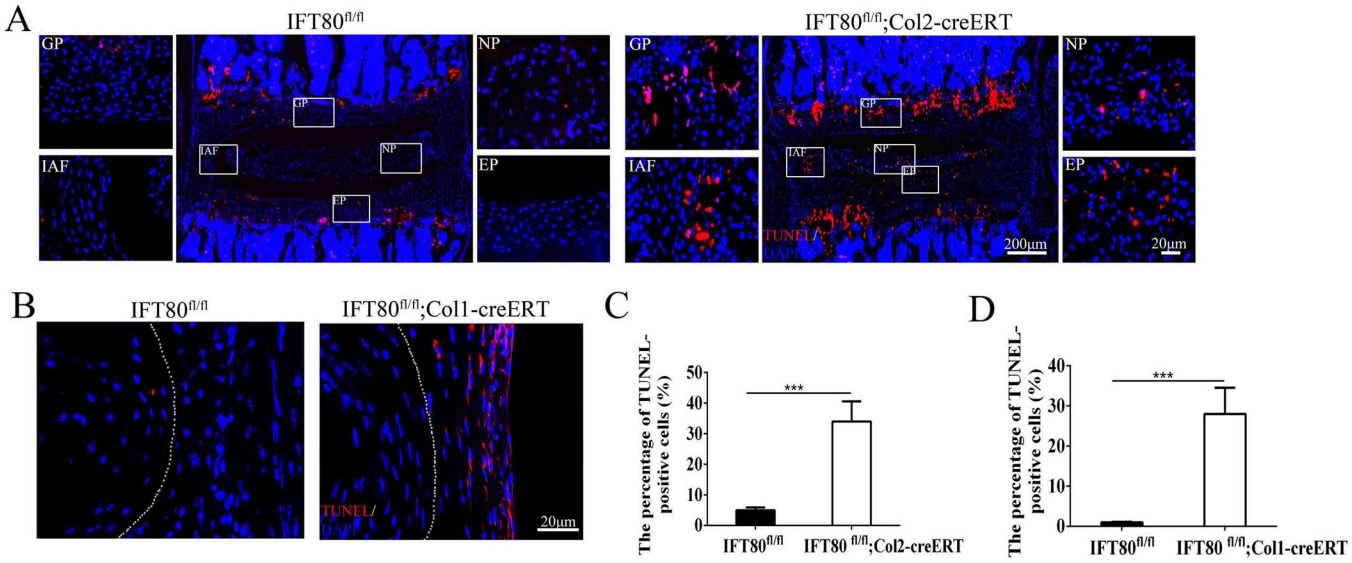

Figure 7.

Deletion of IFT80 promotes cell apoptosis in IVD cells.

(A) TUNEL assay of IFT80$^{fl/fl}$ and IFT80$^{fl/fl}$; Col2-creERT lumbar IVD sections shows increased cell death in the GP, EP, NP and IAF of IFT80$^{fl/fl}$; Col2-creERT mice (central panel). Corresponding high magnification of the area within the box is shown. Red: TUNEL. Blue: DAPI. (B) TUNEL assay of IFT80$^{fl/fl}$ and IFT80$^{fl/fl}$; Col1-creERT IVD sections shows increased cell death in the OAF of IFT80$^{fl/fl}$; Col1-creERT mice. Red: TUNEL. Blue: DAPI. (C) Quantitative analysis of the percentage of TUNEL-positive cells to the total cells per view in (A). (n=3 mice per group). (D) Quantitative analysis of the percentage of TUNEL-positive cells to the total cells per view in (B). (n=3 mice per group). All data are reported as mean ± s.d. Statistical significance was determined by Student's t-test. *P<0.05, **P<0.01, ***P<0.0001. NS = not statistically significant.

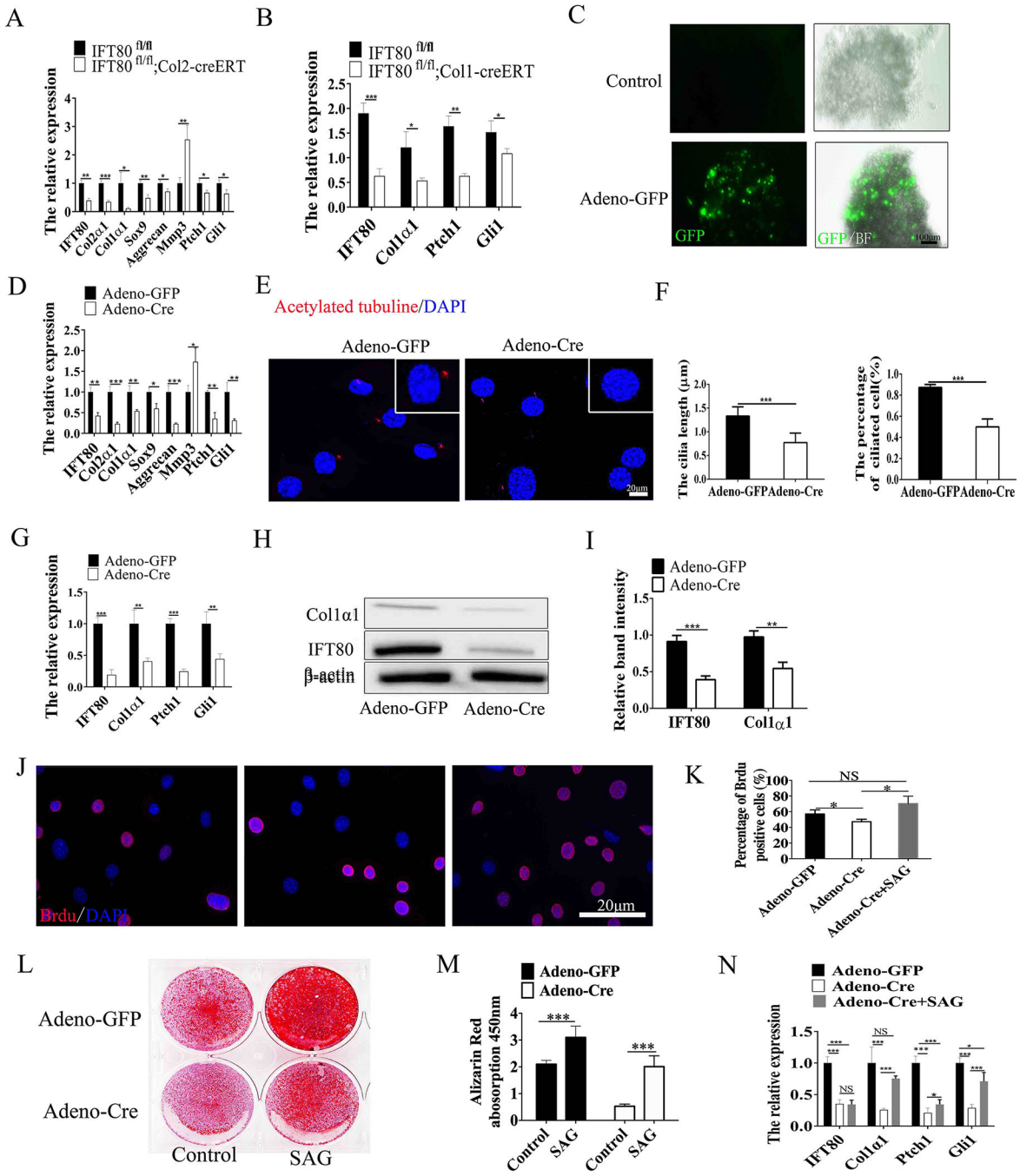

Figure 8.

Deletion of IFT80 decreases the expression levels of cell differentiation markers and Hh signal components in the IVD.

(A) Real-time RT-PCR measurements of IFT80, Col2α1, Col1α1, Sox9, Aggrecan, MMP3, Ptch1 and Gli1 expression levels in the IVD tissue from 4-week-old IFT80$^{fl/fl}$ and IFT80$^{fl/fl}$; Col2-creERT mice. (n=3, triplicates per group). (B) Real-time RT-PCR measurements of IFT80, Col1α1, Ptch1 and Gli1 expression levels in the OAF tissue from 4-week-old IFT80$^{fl/fl}$ and IFT80$^{fl/fl}$; Col1-creERT mice. (n=3, triplicates per group). (C) Fluorescent

images show that adenovirus effectively infected cultured NP tissues. The isolated NP tissues were infected with Ad-GFP for 48 h, and the tissues were examined under fluorescence (GFP) and bright field (BF) to generate the superimposed images (Upper panel represents the control). (D) Real time RT-PCR measurements of IFT80, Col2α1, Col1α1, Sox9, Aggrecan, MMP3, Ptch1 and Gli1 expression level in NP tissues under treatments of Ad-GFP and Ad-Cre. (n=3, triplicates per group). (E) Immunofluorescent staining for acetylated tubulin and DAPI showing the cilia length and percentage in OAF cells from Ad-GFP and Ad-Cre group. Red: Acetylated tubulin, and Blue: DAPI. (F) Quantitative measurements of primary cilia length and percentage of (E). (n=3 with at least 100 cells analyzed) (G) Real time RT-PCR measurements of IFT80, Col1α1, Ptch1 and Gli1 expression levels in OAF cells treated with Ad-GFP and Ad-Cre. (n=3, triplicates per group) (H) Western blot analysis of IFT80 and Col1α1 in OAF cells treated with Ad-GFP and Ad-Cre. (I) Quantitative analysis of the band intensity in (H) (n=3). (J) Immunofluorescent staining for BrdU and DAPI showing the proliferative OAF cells from Ad-GFP or Ad-Cre and treated with SAG group. Red: BrdU, and Blue: DAPI. (K) Quantitative measurements of BrdU positive cells in (E). (n=3; with at least 100 cells analyzed each). (L) Alizarin red staining for osteogenesis differentiation ability of OAF cells from Ad-GFP or Ad-Cre and treated with SAG group. (M) Quantitative of osteogenesis differentiation ability in (E). (n=3, triplicates per group). (N) Real time RT-PCR measurements of IFT80, Col1α1, Ptch1 and Gli1 expression levels in OAF cells treated with Ad-GFP or Ad-Cre and treated with SAG. (n=3, triplicates per group) All data are reported as mean ± s.d. Statistical significance was determined by one-way ANOVA and Student's t-test. *P<0.05, **P<0.01, ***P<0.0001. NS = not statistically significant.

Table 1.

Primer

	Frowd	Revese
IFT80	5’-AAGGAACCAAAGCATCAAGAATTAG-3’	5’-AGATGTCATCAGGCAGCTTGAC-3’
Sox9	5’-TCCCCGCAACAGATCTCCTA-3’	5’-AGGTGGAGTAGAGCCCTGAG-3’
Aggrecan	5’-CGTTGCAGACCAGGAGCAAT-3’	5’-AGGAGTGACAATGCTGCTCA-3’
MMP3	5’-GGCCTGGAACAGTCTTGGC-3’	5’-TGTCCATCGTTCATCATCGTCA-3’
Patch	5’-GACCGGCCTTGCCTCAACCC-3’	5’-CAGGGCGTGAGCGCTGACAA-3’
Glil	5’-GAGTGCCATGCCGCAGCAGA-3’	5’-ACTGGCCCTCCGAGTGACCC-3’
Collai	5’-GCAACAGTCGCTTCACCTACA-3’	5’-CAATGTCCAAGGGAGCCACAT-3’
Col2al	5’-GCAGAATGGGCAGAGGTATAA-3’	5’-AGTCTGGGTCTTCACAGATAAT G-3’
GAPDH	5’-CACATTGGGGGTAGGAACAC-3’	5’-AACTTTGGCATTGTGGAAGG-3’

Table 2.

The cilia length and percentage in intervertebral disc from 4-weeks old mice

	Growth plate	Endplate cartilage	Nucleus pulposus	Annulus fibrosus
Cilia length	0.5-4μm	0.5-4μm	0.5-15μm	0.5-3.5μm
Percentage of ciliated cell	50-80%	30-60%	20-40%	20-50%